Electronic Supplementary Material (ESI) for ChemComm.

Supporting Information

Oxygen-Atom Transfer Photochemistry of a Molecular Copper Bromate Complex

Gerard P. Van Trieste III,[1] Joseph Reibenspies,[1] Yu-Sheng Chen,[2] Debabrata Sengupta,[1] Richard R. Thompson,[1] and David C. Powers[1,*]

[1]*Department of Chemistry, Texas A&M University, College Station, Texas 77843, United States*
[2]*ChemMatCARS, University of Chicago, Argonne, IL 60439, United States*

Email: powers@chem.tamu.edu

Table of Contents

A. General Considerations

SAFETY NOTE. CAUTION: Perchlorate salts can pose an explosion safety risk. No explosions were encountered during the described synthetic and photochemical experiments, but appropriate caution should be exercised when working with perchlorates.

Materials and Methods. Unless otherwise noted, all the chemicals and solvents (ACS reagent grade) were used as received. Potassium bromate, sodium iodide, benzyl alcohol, copper(II) bromide, and sodium perchlorate were purchased from Alfa Aesar. Ammonium persulfate, 2-picolyl amine, cesium carbonate, carbon monoxide, tetrakis(acetonitrile)copper(I) tetrafluoroborate, benzene, and molecular sieves (4 Å, MS) were purchased from Sigma Aldrich. Sodium tetrafluoroborate was purchased from AK Scientific. 2-(Chloromethyl)pyridine hydrochloride was purchased for Matrix Scientific. Cyclohexane, 1,4-cyclohexadiene, iodobenzene diacetate, and styrene were purchased from Acros Organics. 1-Octene was purchased from Oakwood chemical. Cyclohexane, cyclohexadiene, styrene, and 1-octene were dried according to literature methods[1] and subsequently degassed by three free-pump-thaw cycles. N_2, CO, and CO_2 were purchased from Airgas. NMR solvents were obtained from Cambridge Isotope Laboratories were degassed by three free-pump-thaw cycles and were stored over molecular sieve (3 Å) for 24 h prior to use. All reactions were carried out under an ambient atmosphere unless otherwise noted. Anhydrous acetonitrile and toluene were obtained from a drying column and stored over activated molecular sieves.[2] Anhydrous acetonitrile was stored over 3 Å molecular sieves; all other solvents were stored over 4 Å molecular sieves. Tris(2-pyridylmethyl)amine (tpa),[3] silver bromate,[4] and iodosyl benzene (PhIO),[5] were prepared according to literature methods.

Characterization Details. NMR spectra were recorded on Bruker Avance NEO 400 NMR operating at 400.09 MHZ for ^{1}H. The NMR spectra were referenced against residual proteo solvent signal: CD_3CN (1.94 ppm, ^{1}H) and $CDCl_3$ (7.26 ppm, ^{1}H).[6] ^{1}H NMR data are reported as follows: chemical shift (δ, ppm), multiplicity (s (singlet), d (doublet), t (triplet), m (multiplet), br (broad), integration. Solution-phase UV-vis spectra were recorded on an Ocean Optics Flame-S miniature spectrometer with DH-mini UV-Vis-NIR light source (200-900 nm). Solution-phase spectra were blanked against the appropriate solvent. IR spectra were recorded on a Shimadzu FTIR/IRAffinity-1 Spectrometer, were blanked against air, and were determined as the average of 64 scans. *In situ* IR spectra were measured in a KBr pellet with a Bruker VERTEX 70, were blanked against air, and were determined as the average of 64 scans. IR data are reported as follows: wavenumber (cm^{-1}), peak intensity (s, strong; m, medium; w, weak). MALDI data was obtained using a Bruker Microflex LRF MALDI-TOF in reflectron mode. No added matrix was used in the reported MALDI experiments. Mass spectrometry data was recorded on either Orbitrap Fusion™ Tribrid™ Mass Spectrometer or Q Exactive™ Focus Hybrid Quadrupole - Orbitrap™ Mass Spectrometer from Thermo Fisher Scientific. Kinetic isotope effects (k_H/k_D) were determined by integration of

appropriate peaks in the mass spectrum. Atmospheric pressure chemical ionization mass spectrometry (APCI-MS) experiment was performed using a Thermo Scientific Q Exactive Focus. Sample was injected into a 10 μL loop and methanol was used as a mobile phase at a flow rate of 500 μL/min. The Q Exactive Focus APCI source was operated in full MS in positive mode. The mass resolution was tuned to 70000 FWHM at m/z = 200. The discharge current was set at 5 μA, the sheath gas and auxiliary gas flow rates were set to 25 and 5 arbitrary units, respectively, and the auxiliary gas temperature was set to 300 °C. The transfer capillary temperature was held at 250 °C and the S-Lens RF level was set at 50 V. Exactive Series 2.11/Xcalibur 4.02.47 software was used for data acquisition and processing. Elemental analyses were performed in Atlantic Microlab, Inc., Norcross, GA. X-band EPR spectra were recorded on a Bruker ELEXSYS Spectrometer with a cryogen-free in-cavity temperature control system.

Photochemistry Details. *Steady-State Photolysis.* For standard photochemical reactions, a J-young/Schlenk tube was charged with compound [**8**]ClO_4 (1 equiv.), the appropriate substrate (10 equiv.), and CD_3CN. The solution was photolyzed by a Nikon Hg 100 W lamp equipped with a glass filter (335 < λ < 610 nm) for 4-6 d at 23 °C, depending on the substrate. The reaction mixture was subsequently filtered through Celite and the products were characterized by GC/GCMS and ^{1}H NMR spectroscopy. GC retention times were established by comparison with authentic samples of the relevant products.

Analysis of Head-Space Gases. An Agilent Trace 1300GC with attached thermal conductivity detector and a custom-made 120 cm stainless steel column packed with Carbosieve-II was used for analysis of headspace gases. The column was kept at 200 °C and Ar was used as carrier gas. The detector was set to a temperature of 250 °C. Headspace gas (~300 μL) was transferred to the GC with a 0.50 mL Valco Precision Sampling Syringe (Series A-2) equipped with a Valco Precision sampling needle with a 5-point side port.

X-Ray Diffraction Details. X-ray crystal structures of [**8**]ClO_4 before and after photolysis were collected using synchrotron radiation (0.41328 Å) at ChemMatCARS located at the Advanced Photon Source (APS) housed at Argonne National Laboratory (ANL). Crystals suitable for X-ray diffraction were mounted on a glass fiber and data was collected at 100 K (Cryojet N_2 cold stream) using a vertically mounted Bruker D8 three-circle platform goniometer equipped with a PILATUS3 X CdTe 1M detector. Illumination was provided by a Thor Labs 365 nm LED (M365L2) and was delivered to the sample via a 100 μm ID fiber optic. Light intensity was measured with a power meter to be 2 mW at the crystal mount and the spot size of the fiber-delivered light was ~100 μm in diameter. Data were collected as a series of φ and/or ω scans. Data were integrated using SAINT and scaled with a multi-scan absorption correction using SADABS. Structures were solved by intrinsic phasing using SHELXT (Apex2 program suite v2014.1) and refined against F^2 on all data by full matrix least squares with SHELXL97.[7, 8] All non-hydrogen atoms were refined anisotropically. H atoms were placed at idealized positions and refined using a riding model. Refinement details are described in the relevant cif.

Computational Details. Calculations were performed using the Gaussian 16, Revision C.01 suite of software.[9] Geometry optimizations were carried out with the PBE0 functional[10] in conjunction with Grimme's D3 empirical dispersion[11] and Becke-Johnson damping [EMP=GD3BJ],[12] the mod-LANL2DZ basis set[13] and corresponding ECP for Cu,[14] and the 6-311+G* basis set for other atoms;[15] the coordinates for optimized geometries are tabulated in Table S4. Frequency calculations at this level of theory confirmed that optimized geometries represent ground state structures.

B. Synthesis and Characterization

Synthesis of [Cu(tpa)Br]ClO_4 ([**7**]ClO_4)

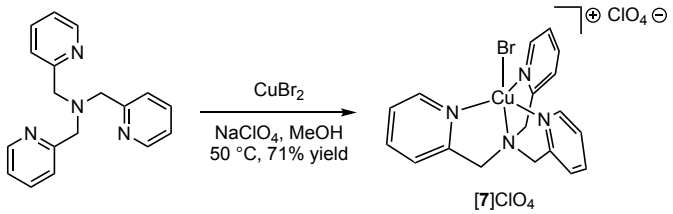

[**7**]ClO_4

[Cu(tpa)Br]ClO_4 ([**7**]ClO_4) was prepared according to the following modification of literature methods.[16] A 100-mL round-bottom flask was charged with tpa (2.92 g, 10.1 mmol, 1.00 equiv.) and methanol (25 mL). The reaction solution was heated to 50 °C. $CuBr_2$ (2.25 g, 10.2 mmol, 1.01 equiv.) was slowly added to the reaction solution and the solution was stirred for 1 h. During this time, the color of the solution became dark green. $NaClO_4$ (1.52 g, 12.5 mmol, 1.24 equiv.) was added as a solid and the reaction mixture was stirred for 15 min. The resulting green precipitate was isolated by hot vacuum filtration. The precipitate was washed with diethyl ether to afford the title compound as a green powder (3.61 g, 71%). Crystals suitable for X-ray diffraction analysis were obtained by slow diffusion of diethyl ether into the acetonitrile solution of the compound. ^{1}H NMR (δ, 23 °C, CD_3CN): 29.8 (br s, 12H), 10.3 (br s, 6H). UV-Vis-NIR (solid) (nm): 258, 340, 988. UV-vis (acetonitrile), λ_{max} (nm, e ($M^{-1}cm^{-1}$)): 330 (18100), 995 (900). HRMS ESI-MS (acetonitrile): calculated for $[M]^+$ = 433.998, observed $[M]^+$ = 433.997. IR (KBr pellet, cm^{-1}): 3067 (m), 2959 (m), 2009 (w), 1607 (s), 1571 (m), 1478 (s), 1430 (s), 1364 (m), 1307 (s), 1260 (s), 1085 (s), 1023 (s), 951 (m), 899 (w), 832 (m), 755 (s), 719 (m), 620 (s), 512 (m), 476 (w), 408 (m). Spectral data are well-matched with those available in the literature.[16]

Synthesis of [Cu(tpa)BrO_3]ClO_4 ([**8**]ClO_4)

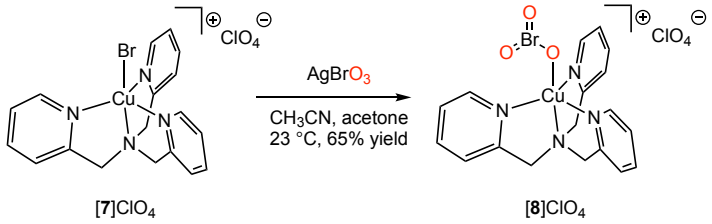

[**7**]ClO_4 [**8**]ClO_4

A 20-mL scintillation vial was charged with [**7**]ClO_4 (2.14 g, 4.04 mmol, 1.00 equiv.), acetone (8 mL), and acetonitrile (2 mL). To that solution, $AgBrO_3$ (2.88 g, 12.3 mmol, 3.07 equiv.) was added and the reaction mixture was stirred in the dark for 24 h at 23 °C. During this time, the color of the reaction mixture became dark blue. Solids were removed by filtration through a pad of Celite and the filtrate was concentrated *in vacuo*. The residue was washed with diethyl ether. The residue was taken up in acetone and slow diffusion of either diethyl ether or pentane into the acetone solution resulted in crystallization of the title compound (1.53 g, 65% yield following crystallization). ^{1}H NMR (δ, 23 °C, CD_3CN): 28.2 (br s, 12H), 10.7

(br s, 6H). IR (KBr pellet, cm^{-1}): 3067 (m), 2923 (s), 2849 (m), 2016 (w), 1606 (s), 1576 (m), 1481 (s), 1437 (s), 1367 (m), 1310 (s), 1266 (s), 1096 (s), 1020 (s), 957 (s), 900 (w), 881 (w), 844 (s), 744 (s), 730 (s), 649 (m), 623 (s), 496 (m), 484 (w), 433 (w). UV-Vis-NIR (solid) (nm): 267, 914. UV-vis (acetone), λ_{max} (nm, ε ($M^{-1}cm^{-1}$)): 426 (2.3×10^1), 710 (3.0×10^2), 920 nm (5.4×10^2). Anal. Calc. for $C_{18}H_{18}N_4O_7BrClCu$: C, 37.19; H, 3.12, N, 9.64. Found C, 37.22; H, 3.15, N, 9.59.

Synthesis of [Cu(tpa)Br]BF_4 ([7]BF_4)

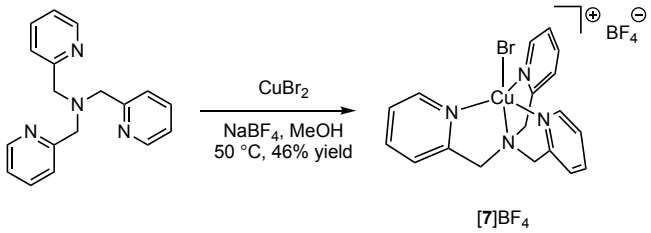

[7]BF_4

[Cu(tpa)Br]BF_4 ([**7**]BF_4) was prepared according to the following modification of literature methods.[16] A 20-mL scintillation vial was charged with tpa (102 mg, 0.353 mmol, 1.00 equiv.) and methanol (1.00 mL). The reaction solution was heated to 50 °C. $CuBr_2$ (78.7 mg, 0.352 mmol, 0.997 equiv.) was slowly added to the reaction solution and the solution was stirred for 1 h. During this time, the color of the solution became dark green. $NaBF_4$ (58.0 mg, 0.532 mmol, 1.51 equiv.) was added as a solid and the reaction mixture was stirred for 15 min. The observed green precipitate was isolated by hot vacuum filtration. The precipitate was washed with diethyl ether to afford the title compound as a green powder (82.0 mg, 46%). NMR (δ, 23 °C, CD_3CN): 30 (br s, 12H), 10.3 (br s, 6H). ^{19}F NMR (δ, 23 °C, CD_3CN): –145 (s, 4F).

Synthesis of [Cu(tpa)BrO_3]BF_4 ([8]BF_4)

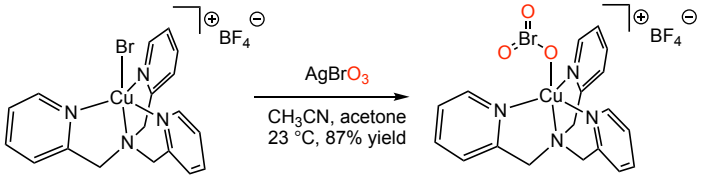

[7]BF_4 [8]BF_4

A 20-mL scintillation vial was charged with [**7**]BF_4 (82.0 mg, 0.158 mmol, 1.00 equiv.), acetone (0.809 mL), and acetonitrile (0.200 mL). $AgBrO_3$ (110 mg, 0.468 mmol, 2.96 equiv.) was added as a solid and the reaction mixture was stirred in the dark for 24 h at 23 °C. During this time, the color of the reaction mixture became dark blue. Solids were removed by filtration through Celite and the filtrate was concentrated *in vacuo*. The residue was washed with diethyl ether affording the title compound (77.0 mg, 87%). ^1H NMR (δ, 23 °C, CD_3CN): 30 (br s, 12H), 10.6 (br s, 6H). ^{19}F NMR (δ, 23 °C, CD_3CN): –150 (s, 4F).

C. Reactivity Studies

Oxygenation of Carbon Monoxide

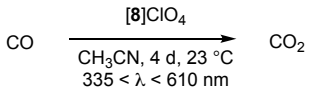

In an N_2-filled glovebox, a J-young tube was charged with [**8**]ClO_4 (40 mg, 0.070 mmol) and dissolved in acetonitrile (0.75 mL). The reaction mixture was degassed by three freeze-pump-thaw cycles and the headspace was refilled with 1 atm of CO. The reaction mixture was photolyzed for 4 d at 23 °C using a 100 W Hg lamp with a 335-610 nm band-pass filter. The reaction headspace was analyzed by gas chromatography (Figure S6), which indicated the formation of CO_2.

Oxidation of 1,4-Cyclohexadiene

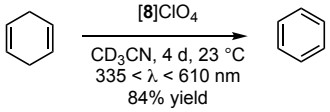

In an N_2-filled glovebox, a J-young tube was charged with [**8**]ClO_4 (40 mg, 0.070 mmol, 1.0 equiv.), cyclohexadiene (0.70 mmol, 10 equiv), and CD_3CN (0.60 mL). The reaction mixture was photolyzed for 4 d at 23 °C using a 100 W Hg lamp with a 335-610 nm band-pass filter. The reaction mixture was filtered through Celite. The resulting solution was analyzed via ^1H NMR (ethylbenzene (10 μL) added as internal standard), which indicated formation of benzene (84%).

Epoxidation of α-Olefins

In an N_2-filled glovebox, a J-young tube was charged with [**8**]ClO_4 (100 mg, 0.180 mmol, 1.00 equiv.), α-olefin (1.80 mmol, 10 equiv), and CD_3CN (2.40 mL). The reaction mixture was photolyzed for 4 d at 23 °C using a 100 W Hg lamp with a 335-610 nm band-pass filter. The resulting mixture was filtered through a pad of Celite and concentrated *in vacuo*. The residue was purified by column chromatography with EtOAc / hexanes system (v/v: 1:10) to afford products **9** (19.0 mg, 91% yield) and **10** (8.3 mg, 36% yield), respectively.

Epoxidation of *cis*-β-Methylstyrene

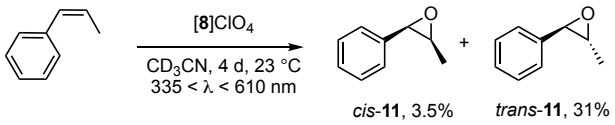

In an N_2-filled glovebox, a Schlenk tube was charged with [**8**]ClO_4 (40 mg, 0.070 mmol, 1.00 equiv.), *cis*-β-methylstyrene (0.70 mmol, 10 equiv), and CD_3CN (0.60 mL). The reaction mixture was photolyzed for 4 d at 23 °C using a 100 W Hg lamp with a 335-610 nm band-pass filter. The resulting solution was analyzed via ^1H NMR (dichloromethane (10 μL) added as internal standard), which indicated formation of *cis*-**11** (3.5%) and *trans*-**11** (31%).

Hydroxylation of Toluene

In an N_2-filled glovebox, a J-young tube was charged with [**8**]ClO_4 (40 mg, 0.070 mmol, 1.0 equiv.), toluene (0.70 mmol, 10 equiv), and CD_3CN (0.60 mL). The reaction mixture was photolyzed for 4 d at 23 °C using a 100 W Hg lamp with a 335-610 nm band-pass filter. The reaction mixture was filtered through a pad of Celite. The resulting solution was analyzed via ^1H NMR (ethylbenzene (10 μL) added as internal standard), which indicated formation of benzyl alcohol (76%).

Determination of the kinetic isotope effect (KIE) of hydroxylation. In an N_2-filled glovebox, a J-young tube was charged with [**8**]ClO_4 (0.040 g, 0.070 mmol, 1.0 equiv.), toluene (0.70 mmol, 10 equiv), toluene-d_8 (0.70 mmol, 10 equiv.), and acetonitrile (0.40 mL). The reaction mixture was photolyzed for 4 d at 23 °C using a 100 W Hg lamp with a 335-610 nm band-pass filter. The reaction mixture was filtered through a pad of Celite and k_H/k_D = 3.4(2) was determined by integration of the APCI-MS data obtained from this solution (Figure S12) The experiment was carried out three times and the reported value is the mean of these trials.

Oxidation of Cyclohexane

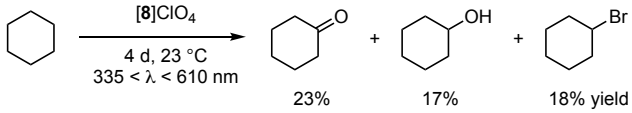

In an N_2-filled glovebox, a J-young tube was charged with [**8**]ClO_4 (100 mg, 0.180 mmol, 1.00 equiv.) and cyclohexane (1.50 mL, 14.5 mmol, 80.5 equiv). The reaction mixture was photolyzed for 6 d at 23 °C using a 100 W Hg lamp with a 335-610 nm band-pass filter. The reaction mixture was filtered through a pad of Celite. The filtrate was purified by column

chromatography with EtOAc / hexanes system (v/v: 3:7) to afford cyclohexanone (4.1 mg, 23% yield), cyclohexanol (3.1 mg, 17% yield), and bromocyclohexane (5.3 mg, 18% yield).

Hydroxylation of Toluene with $[Cu(tpa)BrO_3]BF_4$

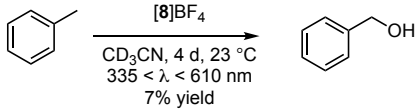

In an N_2-filled glovebox, a Schlenk tube was charged with [**8**]BF_4 (0.038 g, 0.070 mmol, 1.0 equiv.), toluene (0.70 mmol, 10 equiv), and CD_3CN (0.60 mL). The reaction mixture was photolyzed for 4 d at 23 °C using a 100 W Hg lamp with a 335-610 nm band-pass filter. The reaction mixture was filtered through a pad of Celite. The product was analyzed via ^1H NMR (ethylbenzene (10 μL) added as internal standard), which indicated formation of benzyl alcohol (7%).

Epoxidation of *cis*-β-methylstyrene with $[Cu(tpa)]BF_4$

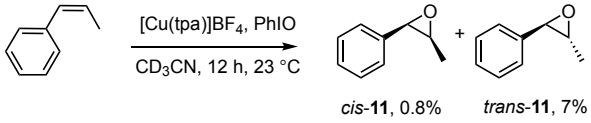

In an N_2-filled glovebox a Schlenk tube was charged with tpa (0.041 g, 0.14 mmol, 1.1 equiv.), $[Cu(MeCN)_4]BF_4$ (0.042 g, 0.13 mmol, 1.0 equiv.), and CD_3CN (0.60 mL). The reaction mixture was stirred for 30 min. PhIO (0.029 g, 0.13 mmol, 1.0 equiv), and cis-β-methylstyrene (0.42 mmol, 3 equiv) were added to the reaction mixture. The resulting reaction mixture was stirred overnight at 23 °C. The product was analyzed via ^1H NMR (dichloromethane (10 μL) added as internal standard), which indicated formation of *cis*-epoxide (0.8%) and *trans*-epoxide (7%). The similarity of the diastereoselection in this experiment to that observed in the photolysis of [**8**]ClO_4 suggests a common reactive oxygen species mediates the processes.

D. **Supporting Data**

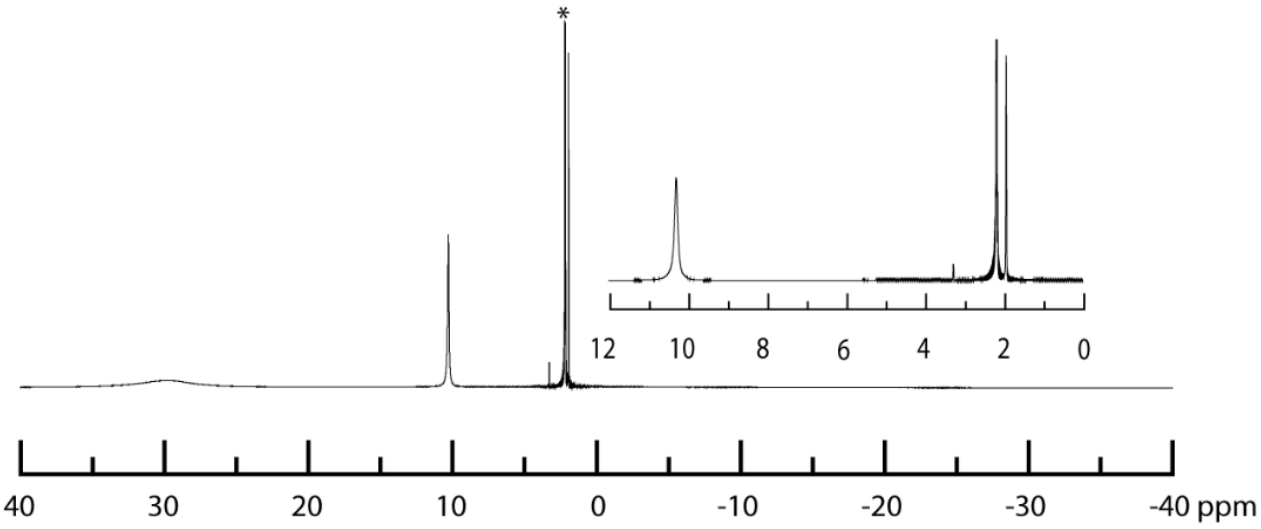

Figure S1. ^{1}H NMR spectrum of [**8**]ClO_4 measured in CD_3CN at 23 °C. The indicated peak [*] corresponds to residual water. Inset: expansion of the 0–12 ppm spectral range.

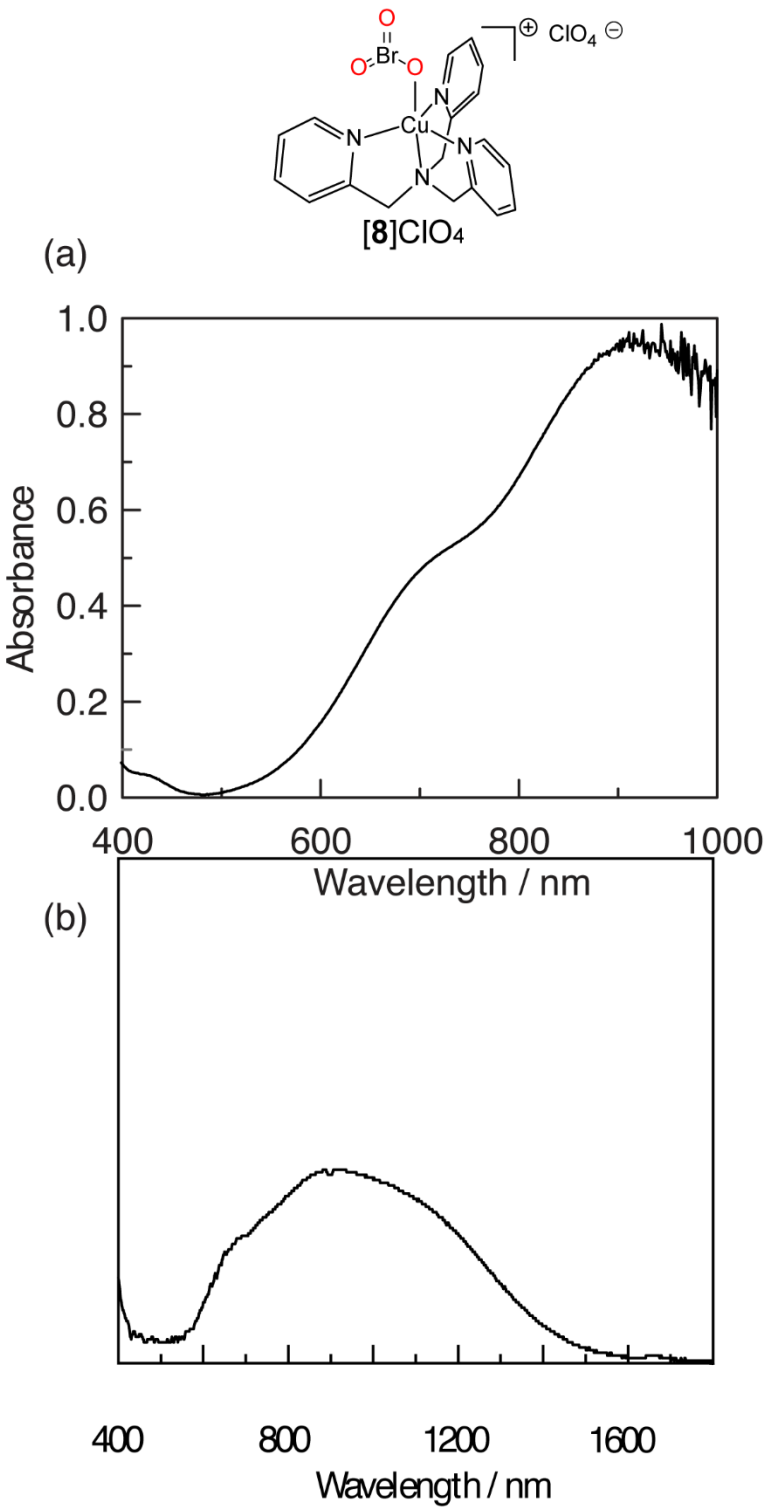

Figure S2. UV-vis spectra of [**8**]ClO_4. (a) UV-vis spectrum of [**8**]ClO_4 measured in acetone at 23 °C. Absorptions are observed at 426 (ε = 2.3 × 10), 710 (ε = 3.0 × 10^2), and 920 nm (ε = 5.4 × 10^2). (b) Diffuse reflectance spectrum of [**8**]ClO_4 measured in the solid-state at 23 °C. Absorptions are observed at 695 nm and 922 nm.

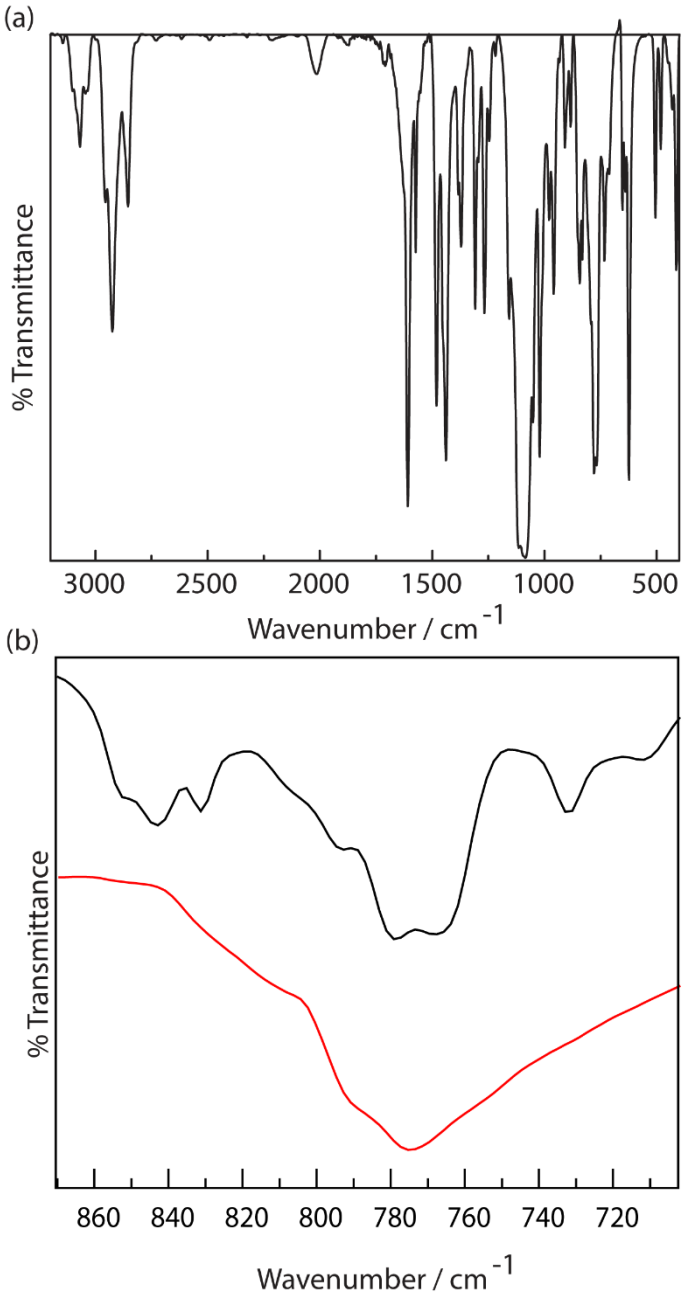

Figure S3. (a) IR spectrum of [**8**]ClO_4 recorded in a KBr pellet at 23 °C. (b) Expansion of spectral window depicting the bromate region. The spectrum of compound [**8**]ClO_4 features peaks at 767 and 778 cm^{-1} (**–**), which are attributed to stretching modes characteristic of the bromate ligand. These features are distinct from those of $KBrO_3$, which are observed at 774 and 790 cm^{-1} (**–**).[17]

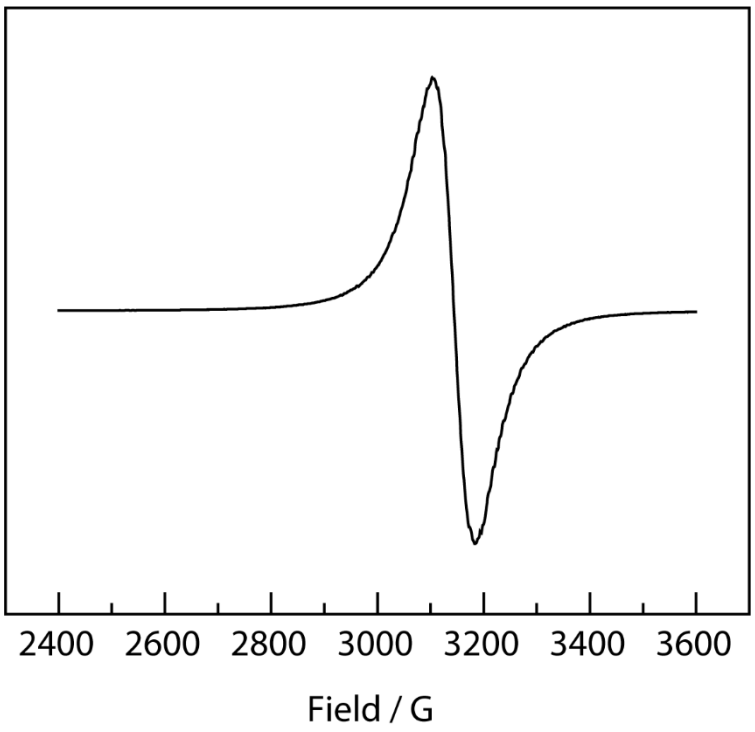

Figure S4. X-band EPR spectrum of [**8**]ClO_4 collected at 4 K in toluene.

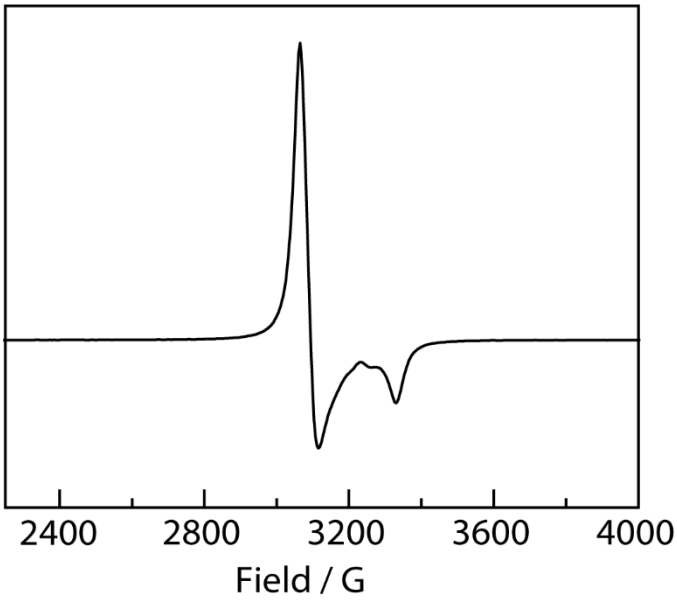

Figure S5. X-band EPR spectrum of [**7**]ClO_4 collected in solution-state (toluene) at 296 K. The observed g-value anisotropy is consistent with either trigonal bipyramidal or distorted octahedral geometry.

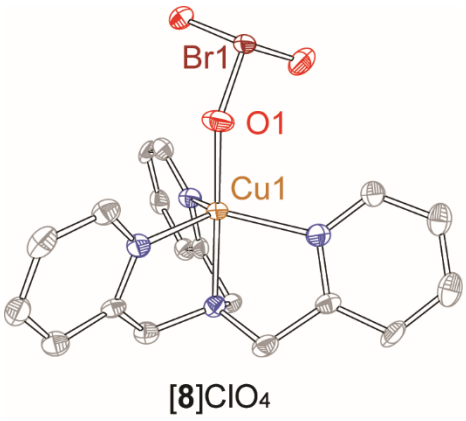

Figure S6. Displacement ellipsoid plot of [**8**]ClO_4 drawn at 50% probability. H-atoms and counter anion are removed for clarity. The crystalline sample used in this diffraction experiment was obtained by slow diffusion of diethyl ether into the acetone solution at 23 °C.

Table S1. X-ray experimental details of [**8**]ClO_4 (CCDC 2178161)

Crystal data	
Chemical formula	$C_{18}H_{18}BrCuN_4O_3 \cdot ClO_4$
M_r	581.26
Crystal system, space group	Triclinic, $P\bar{1}$
Temperature (K)	100
a, b, c (Å)	9.4468(6), 14.4723(9), 15.792(1)
α, β, γ (°)	83.285(1), 80.507(1), 89.649(1)
V (Å^3)	2114.6(2)
Z	4
Radiation type	Synchrotron, λ = 0.41328 Å
μ (mm^{-1})	0.72
Crystal size (mm)	0.02 × 0.02 × 0.01
Data collection	
Diffractometer	Bruker
Absorption correction	Multi-scan SADABS2016/2 (Bruker,2016/2) was used for absorption correction. wR2(int) was 0.1097 before and 0.0813 after correction. The Ratio of minimum to maximum transmission is 0.8593. The λ/2 correction factor is Not present.
T_{min}, T_{max}	0.859, 1.000
No. of measured, independent and observed [I > 2s(I)] reflections	45899, 8155, 6474
R_{int}	0.066
(sin θ/λ)$_{max}$ (Å^{-1})	0.632
Refinement	
R[F^2 > 2s(F^2)], wR(F^2), S	0.047, 0.130, 1.06
No. of reflections	8155
No. of parameters	578
H-atom treatment	H-atom parameters constrained
Γ$_{max}$, Γ$_{min}$ (e Å^{-3})	1.27, –1.38

Table S2. Relevant X-ray metical parameters of [**8**]ClO_4 and other [Cu(tpa)X] complexes that feature apical oxyanions.

Entry	reference	Cu–$N_{pyridine}$ / Å	Cu–N_{amine} / Å	Cu–O / Å
[**8**]ClO_4	this work	2.072(4)	2.023(3)	1.951(3)
$[Cu(tpa)NO_2]^+$	18	2.0741(3)	2.0399(2)	1.931(1)
$[(Cu(tpa))_2C_4O_4]^{2+}$	19	2.067(4)	2.005(4)	1.944(3)
$[(Cu(tpa))_2pyzdc]^{2+}$	20	2.0514(2)	2.0360(2)	1.9343(1)
$[(Cu(tpa))_2N_2O_2]^{2+}$	21	2.0678(2)	2.0572(2)	1.9114(1)
$[Cu(tpa)NO_2]^+$	22	2.076(6)	2.026(5)	1.935(6)
$[Cu(tpa)(BF)]^+$	23	2.071(2)	2.034(2)	1.932(2)

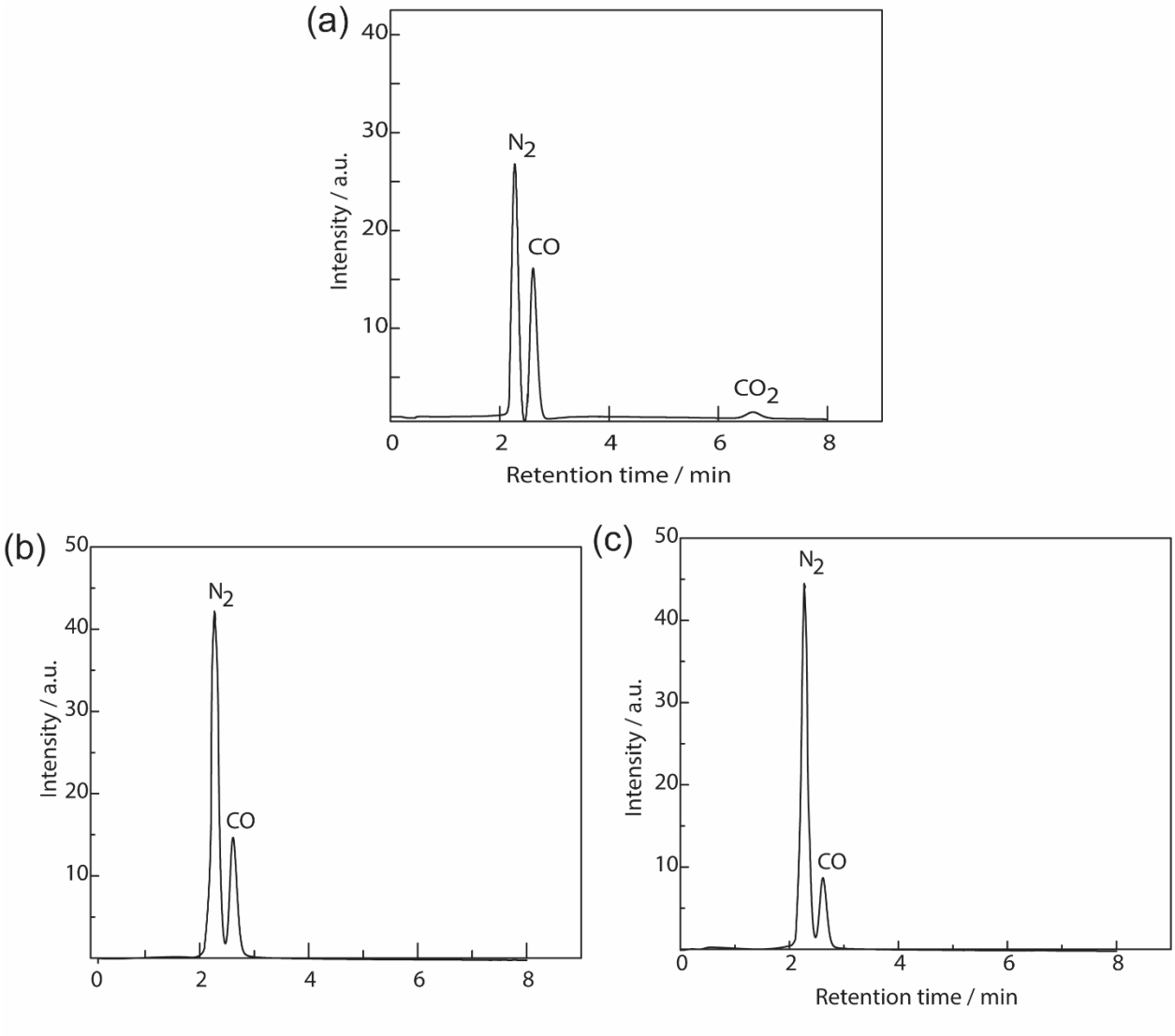

Figure S7. Gas chromatograms (GC) of the headspace of reactions after 4 d photolysis (335 < λ < 610 nm) (a) Photolysis of [**8**]ClO_4 dissolved in CH_3CN in the presence of CO results in the formation of CO_2. GC analysis of the headspace of the reaction shows N_2, CO, and CO_2.(b) Photolysis of a CH_3CN solution in the presence of CO. GC analysis of the headspace of the reaction shows only N_2 and CO. (c) Photolysis of $KBrO_3$ dissolved in CH_3CN in the presence of CO. GC analysis of the headspace of the reaction shows only N_2 and CO.

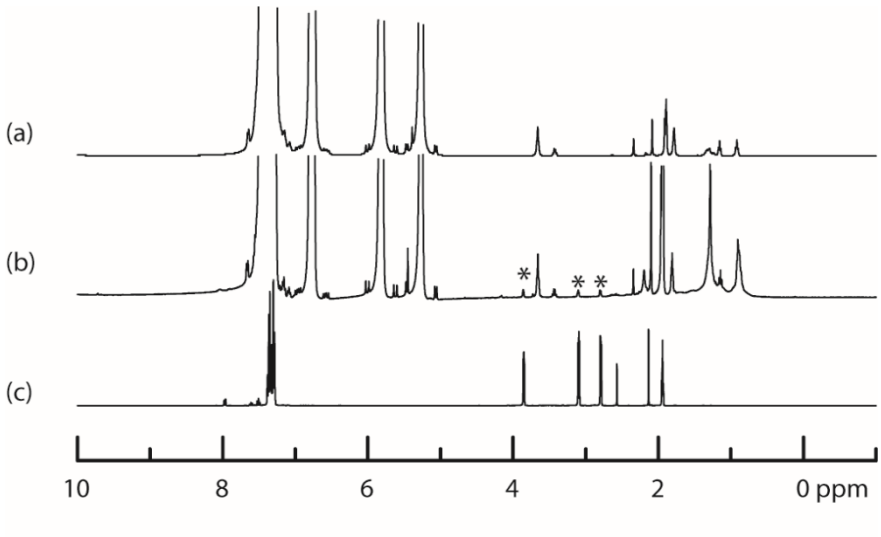

Figure S8. Photolysis ($335 < \lambda < 610$ nm) of [**8**]ClO_4 in CD_3CN and styrene results in the formation of styrene oxide (**9**). (a) ^1H NMR spectrum of the reactant mixture of [**8**]ClO_4 and styrene; (b) ^1H NMR spectrum of the product mixture following photolysis of [**8**]ClO_4; (c) ^1H NMR spectrum of isolated **9** (spectral features attributed to styrene oxide (**9**) marked with *).

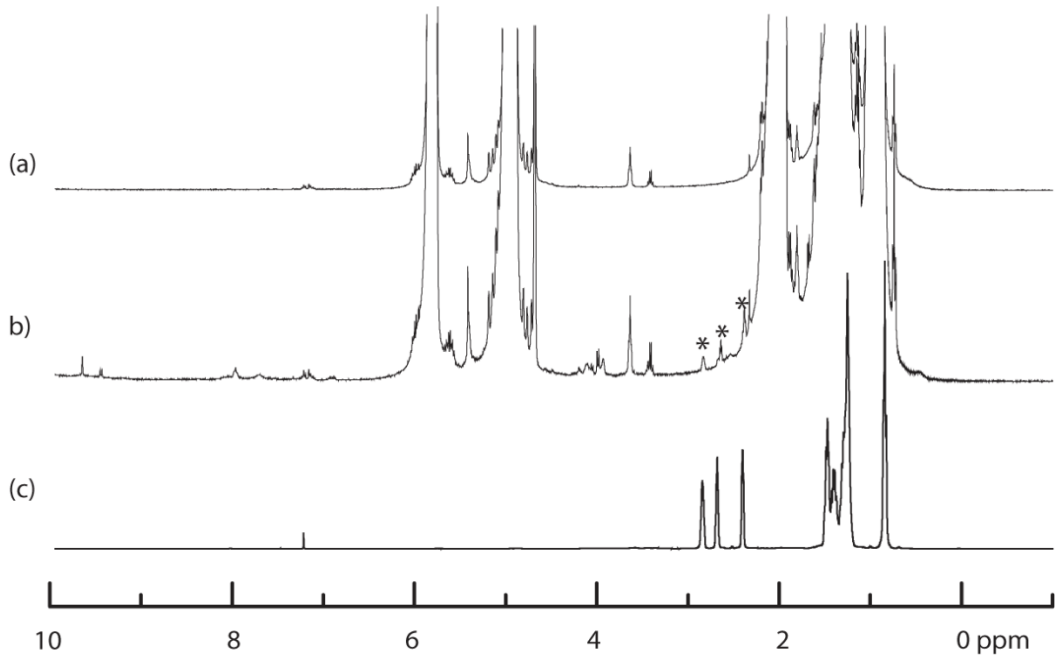

Figure S9. Photolysis (335 < λ < 610 nm) of [**8**]ClO_4 in CD_3CN and 1-octene results in the formation of epoxide **10**. (a) ^1H NMR spectrum of the reactant mixture of [**8**]ClO_4 and 1-octene; (b) ^1H NMR spectrum of the product mixture following photolysis of [**8**]ClO_4; (c) ^1H NMR spectrum of isolated **10** (spectral features attributed to epoxide **10** marked with *).

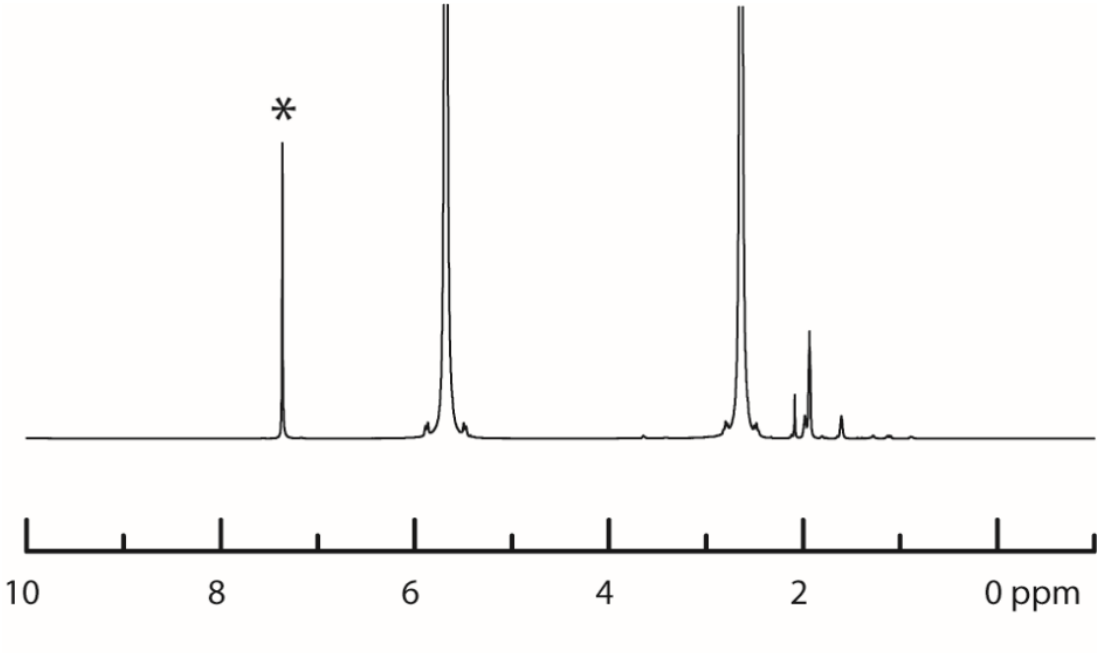

Figure S10. Photolysis (335 < λ < 610 nm) of [**8**]ClO_4 in CD_3CN and 1,4-cyclohexadiene results in the formation of benzene. ^1H NMR spectrum of the product mixture following photolysis of [**8**]ClO_4 (spectral features attributed to benzene marked with *).

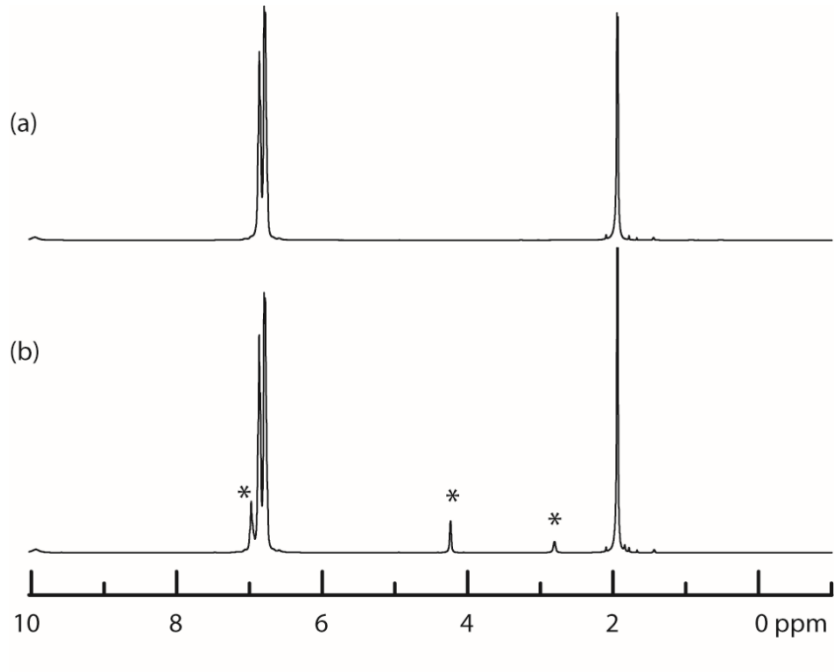

Figure S11. Photolysis ($335 < \lambda < 610$ nm) of [**8**]ClO_4 in CD_3CN and toluene results in the formation of benzyl alcohol. (a) ^1H NMR spectrum of the reactant mixture of [**8**]ClO_4 and toluene; (b) ^1H NMR spectrum of the product mixture following photolysis of [**8**]ClO_4 (spectral features attributed to benzyl alcohol marked with *).

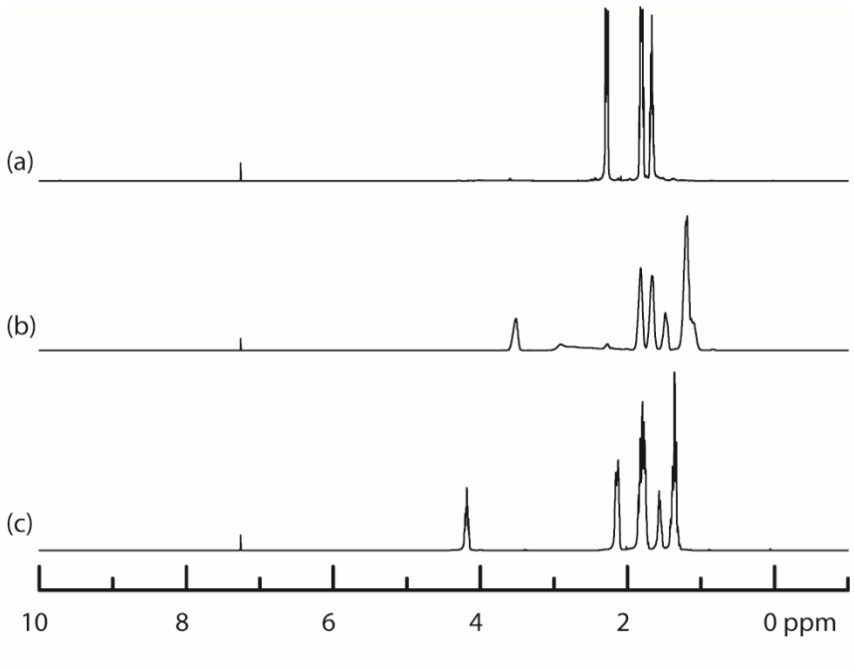

Figure S12. Photolysis ($335 < \lambda < 610$ nm) of [**8**]ClO_4 in cyclohexane results in the formation of cyclohexanone, cyclohexanol, and bromocyclohexane. (a) ^{1}H NMR spectrum of isolated cyclohexanone; (b) ^{1}H NMR spectrum of isolated cyclohexanol; (c) ^{1}H NMR spectrum of isolated bromocyclohexane.

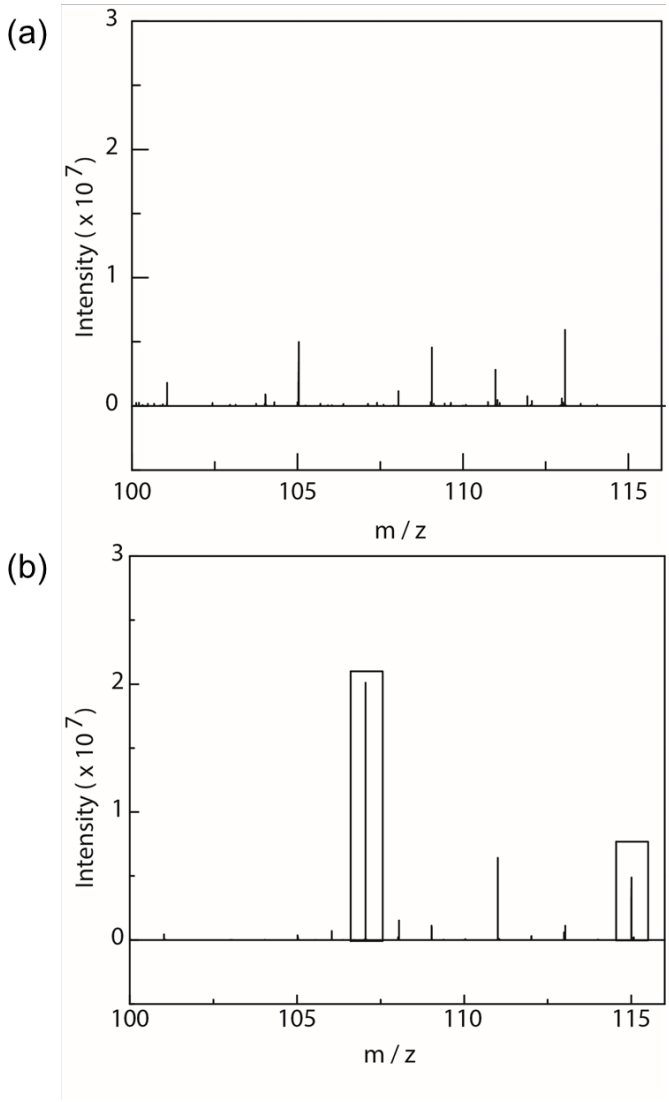

Figure S13. APCI-MS trace for the intermolecular KIE determination. The m/z of benzylalcohol ($C_7H_7O^-$, APCI negative) is 107.0489; the m/z of deuterated benzylalcohol ($C_7D_7O^-$, APCI negative) is 115.0024. (a) The m/z spectrum of the reaction mixture without photolysis which indicates no traces of benzyl alcohols ($C_7H_7O^-$ or $C_7D_7O^-$). (b) The m/z spectrum of the reaction mixture after photolysis (335 < λ < 610 nm) which indicates the characteristic peaks of both benzyl alcohols which was used to calculate the k_H/k_D using the following equation.

$$Intermolecular\ KIE = \frac{Area\ of\ benzyl\ alcohol\ (107.0489)}{Area\ of\ deuterated\ benzyl\ alcohol\ (115.0024)}\ X\ \frac{D8-toluene}{H8-toluene}$$

Sample	Substrate	Average KIE*
[**8**]ClO_4	H8-toluene/D8-toluene	3.4 ± 0.2

* The reaction was performed in triplicate.

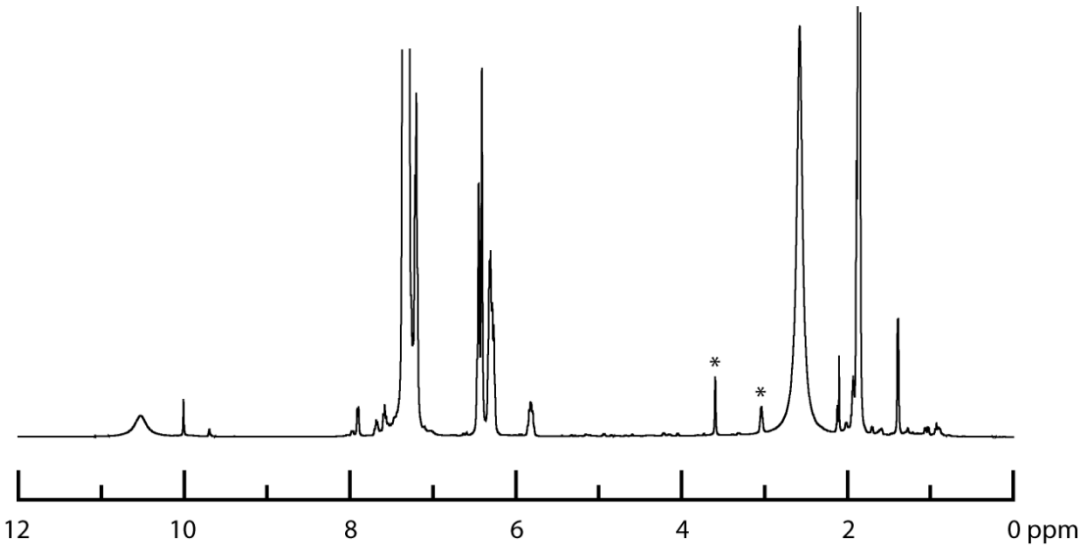

Figure S14. Photolysis (335 < λ < 610 nm) of [**8**]ClO_4 in CD_3CN and *cis*-β-methylstyrene results in the formation of *cis*-**11** and *trans*-**11**. ^1H NMR spectrum of the product mixture following photolysis of [**8**]ClO_4 (spectral features attributed to *trans*-**11** marked with *).

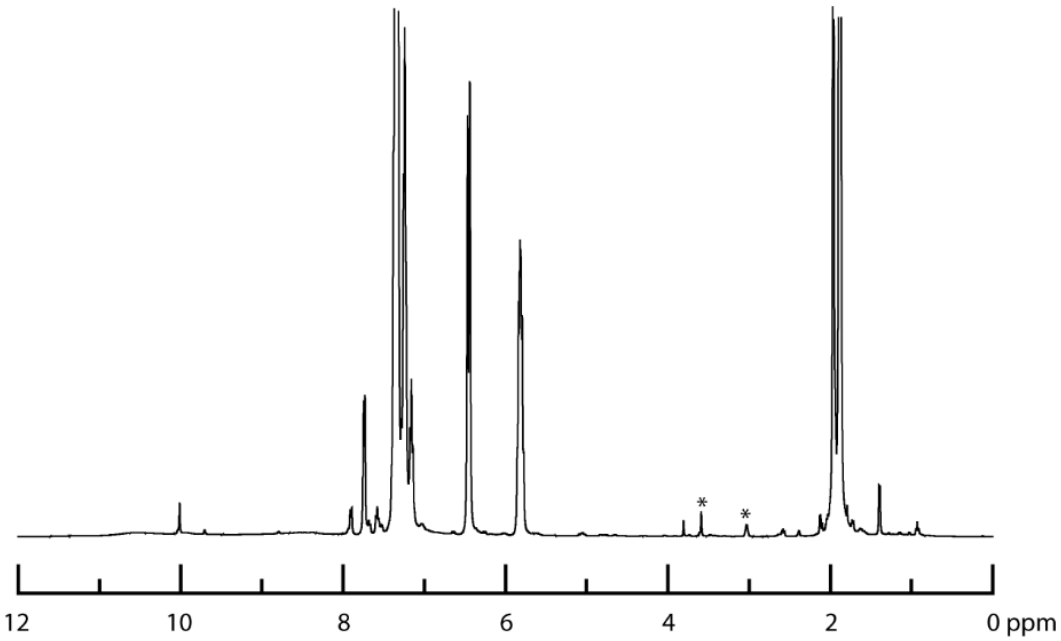

Figure S15. Combination of [Cu(tpa)]BF_4 ([**12**]BF_4), PhIO, and *cis*-β-methylstyrene in CD_3CN results in epoxidation. ^1H NMR spectrum of the crude product mixture (spectral features attributed to *trans*-**11** are marked with *).

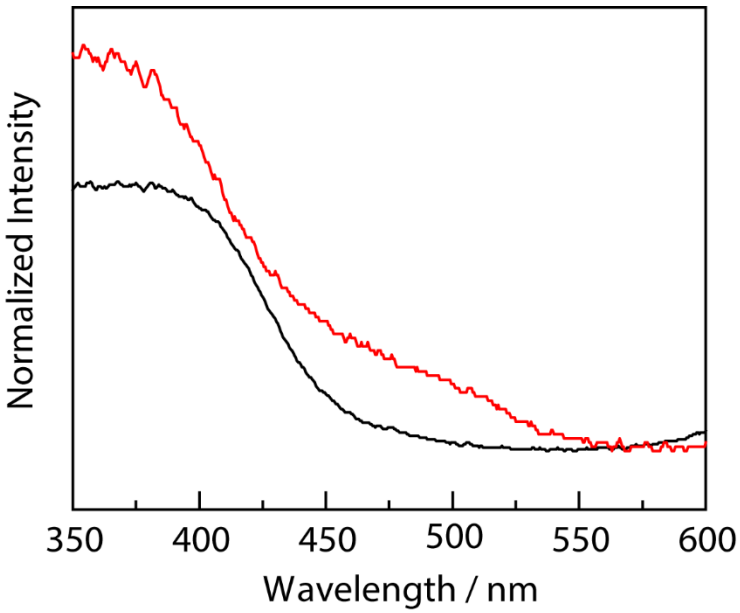

Figure S16. Diffuse reflectance spectrum measured at 23 °C on a KBr pellet sample of [**8**]ClO_4 (black) and the product mixture after 24 h of photolysis (335 < λ < 610 nm). A new absorption centered at 475 nm grows in and is consistent with BrO_2 which has previously been observed in solution-state UV-Vis experiments.[24, 25]

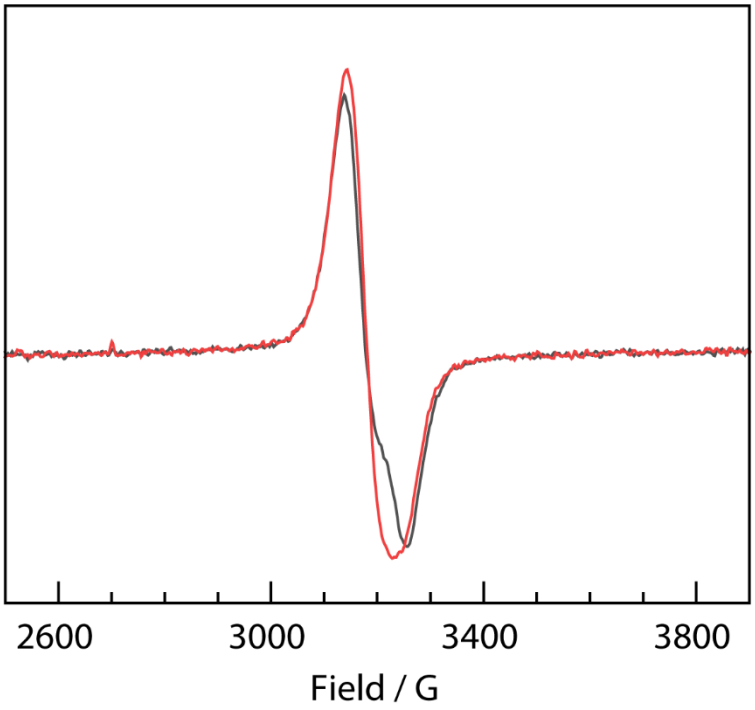

Figure S17. X-band EPR spectrum of [**8**]ClO_4 collected at 296 K in the solid-state (black) and after 2 days of photolysis (red). The minimal changes in both intensity and spectral features are consistent with regeneration of Cu(II) after the photochemistry has taken place. We ascribe this to a series of events involving (a) photoreduction to generate Cu(I) and BrO_3 radical (b) electron-transfer from these resulting species to generate Cu(II) cation and BrO_3 anion (c) recombination of the ions, facilitated by the tight packing of the crystalline lattice. The nearly identical linewidth above the baseline but broader linewidth below for the photolyzed sample as compared to the starting material, suggests a decrease in g-value anisotropy but retention of the $(3d_{z^2})^1$ ground state configuration.

Table S3. X-ray experimental details of [**8**]ClO_4 following photolysis (CCDC 2178160)

Crystal data	
Chemical formula	$C_{18}H_{18}BrCuN_4O_3 \cdot ClO_4$
M_r	581.26
Crystal system, space group	Triclinic, $P\bar{1}$
Temperature (K)	100
a, b, c (Å)	9.424(1), 14.590(2), 15.753(2)
α, β, γ (°)	84.606(2), 80.963(2), 89.819(2)
V (Å^3)	2129.5(4)
Z	4
Radiation type	Synchrotron, λ = 0.41328 Å
μ (mm^{-1})	0.72
Crystal size (mm)	0.02 × 0.02 × 0.01
Data collection	
Diffractometer	Bruker APEX-II CCD
Absorption correction	Multi-scan SADABS2016/2 (Bruker,2016/2) was used for absorption correction. wR2(int) was 0.0965 before and 0.0580 after correction. The Ratio of minimum to maximum transmission is 0.8552. The λ/2 correction factor is Not present.
T_{min}, T_{max}	0.636, 0.744
No. of measured, independent and observed [$I > 2s(I)$] reflections	13380, 4093, 3232
R_{int}	0.053
θ_{max} (°)	11.9
$(\sin\theta/\lambda)_{max}$ (Å^{-1})	0.499
Refinement	
$R[F^2 > 2s(F^2)]$, $wR(F^2)$, S	0.090, 0.276, 1.07
No. of reflections	4093
No. of parameters	577
H-atom treatment	H-atom parameters constrained $w = 1/[\sigma^2(F_o^2) + (0.1693P)^2 + 18.6438P]$ where $P = (F_o^2 + 2F_c^2)/3$
$\Delta\rho_{max}$, $\Delta_{\rho min}$ (e Å^{-3})	1.15, −1.38

Table S4. X,Y,Z coordinates for the optimized geometry of $Cu(tpa)^+$ computed as a singlet at the PBE0 level of theory with mod-LANL2DZ (Cu) and 6-31G(d,p) (light atoms) basis sets.

Atom	X	Y	Z
Cu	0.000284	0.000424	−0.894740
N	−1.615400	1.244599	−0.585320
N	1.885810	0.776376	−0.585210
N	−0.270550	−2.020920	−0.585250
N	−0.000052	0.000397	1.329712
C	−1.763100	1.605402	0.703055
C	−2.881230	2.305940	1.144384
H	−2.972980	2.569650	2.195162
C	−3.867180	2.662680	0.228629
H	−4.747680	3.211725	0.553126
C	−3.707000	2.297796	−1.103920
H	−4.449040	2.549647	−1.855820
C	−2.568280	1.585744	−1.461050
H	−2.406130	1.270006	−2.488930
C	2.271832	0.724013	0.703250
C	3.437905	1.341464	1.144610
H	3.711924	1.289252	2.195459
C	4.240470	2.016074	0.228784
H	5.156477	2.503580	0.553289
C	3.844708	2.059585	−1.103870
H	4.434363	2.575598	−1.855830
C	2.658315	1.430191	−1.461030
H	2.303976	1.447577	−2.488960
C	−0.508930	−2.328990	0.703211
C	−0.556790	−3.647510	1.144751
H	−0.739080	−3.858630	2.195606
C	−0.373330	−4.679920	0.229076
H	−0.408770	−5.716930	0.553713
C	−0.137730	−4.359000	−1.103580
H	0.014732	−5.127690	−1.855430
C	−0.090090	−3.016870	−1.460900
H	0.102130	−2.718750	−2.488860
C	−0.631180	1.267180	1.653410
H	0.135052	2.049213	1.552387
H	−0.991630	1.311382	2.695018
C	1.412489	−0.086580	1.653656
H	1.706389	−1.141270	1.552894
H	1.630944	0.203673	2.695218

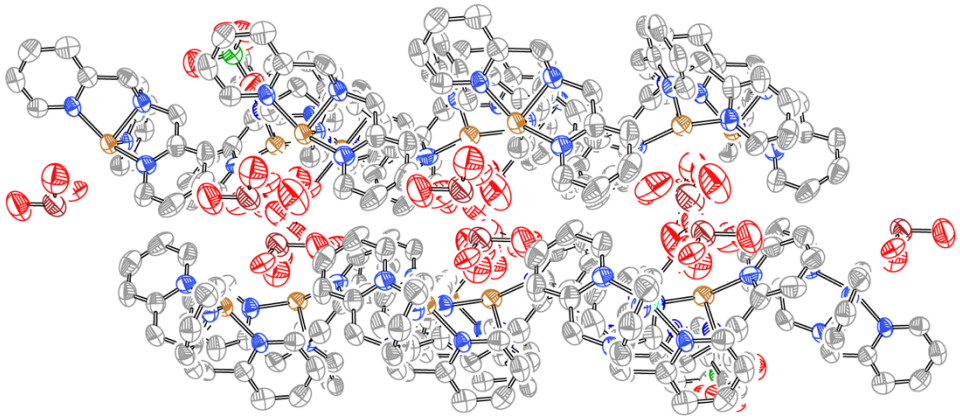

Figure S18. Packing diagram for [**8**]ClO_4 following photolysis that illustrates the close-packed, dense array of BrO_3 fragments.

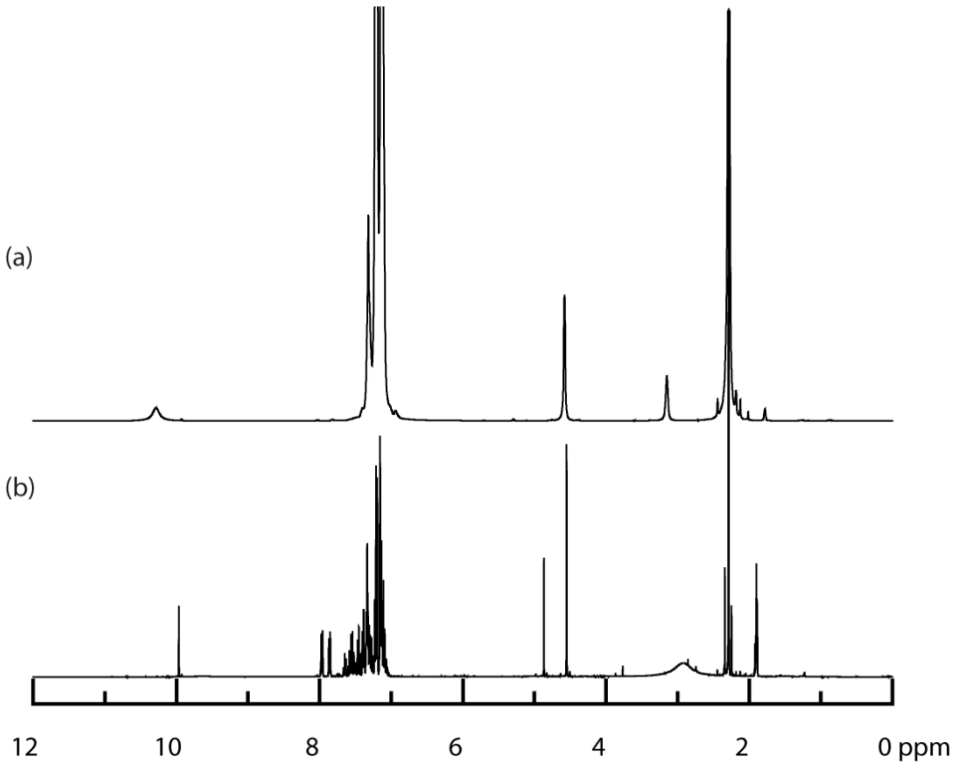

Figure S19. Photolysis (white light) of $KBrO_3$ and $(NH_4)_2S_2O_8$ in CD_3CN and toluene results in formation of benzyl alcohol, benzaldehyde, and benzoate. (a) ^1H NMR spectrum of the product mixture following photolysis of [**8**]ClO_4; (b) ^1H NMR spectrum of the crude product mixture following photolysis of $KBrO_3$ and $(NH_4)_2S_2O_8$ in CD_3CN and toluene.

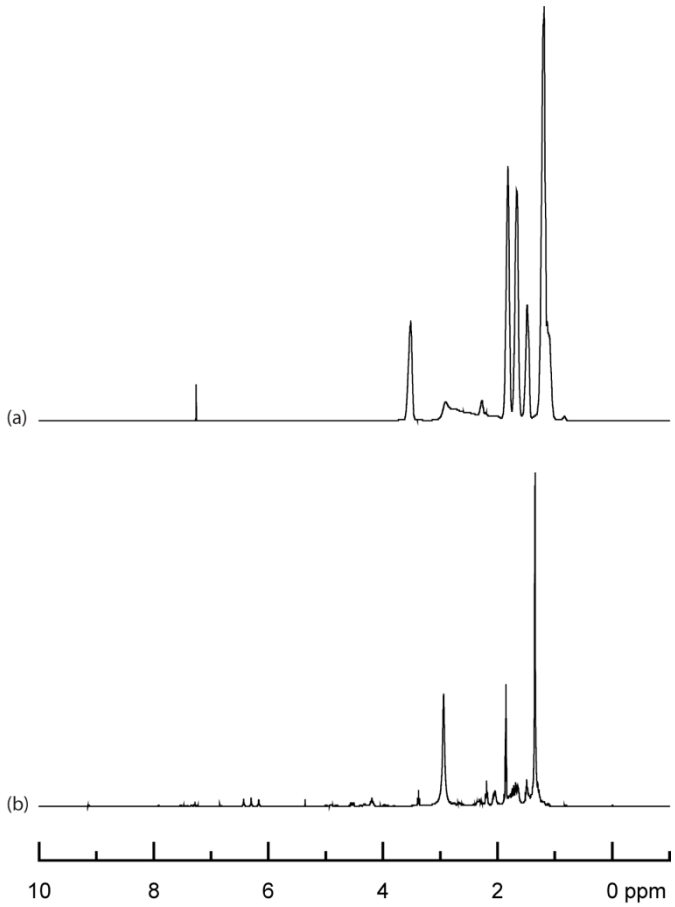

Figure S20. Photolysis (white light) of $KBrO_3$ and $(NH_4)_2S_2O_8$ in CD_3CN and cyclohexane results in formation of cyclohexanol and cyclohexanone. (a) ^1H NMR spectrum of the product mixture following photolysis of [**8**]ClO_4; (b) ^1H NMR spectrum of the crude product mixture following photolysis of $KBrO_3$ and $(NH_4)_2S_2O_8$ in CD_3CN and cyclohexane. While photolysis of [**8**]ClO_4 in the presence of cyclohexane resulted in relatively clean formation of cyclohexanol and cyclohexanone in yields of 17% and 23%, respectively; subjecting $KBrO_3$ and $(NH_4)_2S_2O_8$ to similar conditions resulted in a complex mixture of both oxidized and unsaturated products.

E. References

1. Armarego, W. L. F.; Chai, C. *Purification of Laboratory Chemicals, 5th Edition*. Butterworth-Heinemann: 2003.
2. Pangborn, A. B.; Giardello, M. A.; Grubbs, R. H.; Rosen, R. K.; Timmers, F. J. Safe and Convenient Procedure for Solvent Purification. *Organometallics* **1996**, *15*, 1518.
3. Ward, A. L.; Elbaz, L.; Kerr, J. B.; Arnold, J. Nonprecious Metal Catalysts for Fuel Cell Applications: Electrochemical Dioxygen Activation by a Series of First Row Transition Metal Tris(2-pyridylmethyl)amine Complexes. *Inorg. Chem.* **2012**, *51*, 4694–4706.
4. Song, L.; Li, T.; Zhang, S. Synthesis and characterization of $Ag/AgBrO_3$ photocatalyst with high photocatalytic activity. *Mater. Chem. Phys.* **2016**, *182*, 119–124.
5. Maity, A.; Hyun, S.-M.; Powers, D. C. Oxidase catalysis via aerobically generated hypervalent iodine intermediates. *Nat. Chem.* **2018**, *10*, 200–204.
6. Fulmer, G. R.; Miller, A. J. M.; Sherden, N. H.; Gottlieb, H. E.; Nudelman, A.; Stoltz, B. M.; Bercaw, J. E.; Goldberg, K. I. NMR Chemical Shifts of Trace Impurities: Common Laboratory Solvents, Organics, and Gases in Deuterated Solvents Relevant to the Organometallic Chemist. *Organometallics* **2010**, *29*, 2176–2179.
7. Sheldrick, G. A short history of SHELX. *Acta Cryst. A* **2008**, *64*, 112–122.
8. Sheldrick, G. Crystal structure refinement with SHELXL. *Acta Cryst. C* **2015**, *71*, 3–8.
9. Frisch, M. J.; Trucks, G. W.; Schlegel, H. B.; Scuseria, G. E.; Robb, M. A.; Cheeseman, J. R.; Scalmani, G.; Barone, V.; Petersson, G. A.; Nakatsuji, H.; Li, X.; Caricato, M.; Marenich, A. V.; Bloino, J.; Janesko, B. G.; Gomperts, R.; Mennucci, B.; Hratchian, H. P.; Ortiz, J. V.; Izmaylov, A. F.; Sonnenberg, J. L.; Williams; Ding, F.; Lipparini, F.; Egidi, F.; Goings, J.; Peng, B.; Petrone, A.; Henderson, T.; Ranasinghe, D.; Zakrzewski, V. G.; Gao, J.; Rega, N.; Zheng, G.; Liang, W.; Hada, M.; Ehara, M.; Toyota, K.; Fukuda, R.; Hasegawa, J.; Ishida, M.; Nakajima, T.; Honda, Y.; Kitao, O.; Nakai, H.; Vreven, T.; Throssell, K.; Montgomery Jr., J. A.; Peralta, J. E.; Ogliaro, F.; Bearpark, M. J.; Heyd, J. J.; Brothers, E. N.; Kudin, K. N.; Staroverov, V. N.; Keith, T. A.; Kobayashi, R.; Normand, J.; Raghavachari, K.; Rendell, A. P.; Burant, J. C.; Iyengar, S. S.; Tomasi, J.; Cossi, M.; Millam, J. M.; Klene, M.; Adamo, C.; Cammi, R.; Ochterski, J. W.; Martin, R. L.; Morokuma, K.; Farkas, O.; Foresman, J. B.; Fox, D. J. *Gaussian 16 Rev. C.01*, Wallingford, CT, 2016.
10. Adamo, C.; Barone, V. Toward reliable density functional methods without adjustable parameters: The PBE0 model. *J. Chem. Phys.* **1999**, *110*, 6158–6170.
11. Grimme, S. Semiempirical GGA-type density functional constructed with a long-range dispersion correction. *J. Comput. Chem.* **2006**, *27*, 1787–1799.
12. Grimme, S.; Ehrlich, S.; Goerigk, L. Effect of the damping function in dispersion corrected density functional theory. *J. Comput. Chem.* **2011**, *32*, 1456 01501465.
13. Couty, M.; Hall, M. B. Basis sets for transition metals: Optimized outer p functions. *J. Comput. Chem.* **1996**, *17*, 1359–1370.
14. Hay, P. J.; Wadt, W. R. Ab initio effective core potentials for molecular calculations. Potentials for K to Au including the outermost core orbitals. *J. Chem. Phys* **1985**, *82*, 299–310.
15. Hehre, W. J.; Ditchfield, R.; Pople, J. A. Self—Consistent Molecular Orbital Methods. XII. Further Extensions of Gaussian—Type Basis Sets for Use in Molecular Orbital Studies of Organic Molecules. *J. Chem. Phys.* **1972**, *56*, 2257–2261.
16. Eckenhoff, W. T.; Pintauer, T. Structural Comparison of Copper(I) and Copper(II) Complexes with Tris(2-pyridylmethyl)amine Ligand. *Inorg. Chem.* **2010**, *49*, 10617–10626.
17. Wurzenberger, M. H. H.; Szimhardt, N.; Stierstorfer, J. Nitrogen-Rich Copper(II) Bromate Complexes: an Exotic Class of Primary Explosives. *Inorg. Chem.* **2018**, *57*, 7940–7949.
18. Hematian, S.; Siegler, M. A.; Karlin, K. D. Heme/Copper Assembly Mediated Nitrite and Nitric Oxide Interconversion. *J. Am. Chem. Soc.* **2012**, *134*, 18912–18915.

19. Massoud, S. S.; Mautner, F. A.; Vicente, R.; Louka, F. R. μ-1,3-(trans) and μ-1,2-(cis) Bonding in Squarato-Bridged Dinuclear Copper(II) and Nickel(II) Complexes Derived from Polypyridyl Amines. *Eur. J. Inorg. Chem.* **2008**, 3709–3717.
20. Massoud, S. S.; Deifik, P. J.; Bankole, P. K.; Lalancette, R.; Yee, G. T.; Tatum, D.; Bernal, I.; Mautner, F. A. Structural and magnetic characterization of a novel series of dinuclear Cu(II) complexes bridging by 2,5-pyrazine dicarboxylate. *Inorg. Chim. Acta.* **2010**, *363*, 1001–1007.
21. Wijeratne, G. B.; Hematian, S.; Siegler, M. A.; Karlin, K. D. Copper(I)/NO(g) Reductive Coupling Producing a trans-Hyponitrite Bridged Dicopper(II) Complex: Redox Reversal Giving Copper(I)/NO(g) Disproportionation. *J. Am. Chem. Soc.* **2017**, *139*, 13276–13279.
22. Mukhopadhyay, U.; Bernal, I.; Massoud, S. S.; Mautner, F. A. Syntheses, structures and some electrochemistry of Cu(II) complexes with tris[(2-pyridyl)methyl]amine: $[Cu\{N(CH_2\text{-}py)_3\}(N_3)]ClO_4$ (I), $[Cu\{N(CH_2\text{-}py)_3\}(O–NO)]ClO_4$ (II) and $[Cu\{N(CH_2\text{-}py)_3\}(NCS)]ClO_4$ (III). *Inorg. Chim. Acta.* **2004**, *357*, 3673–3682.
23. Zheng, H.; Que, L. Cu(II)-α-keto acid complexes as structural models of α-keto acid-dependent enzymes: syntheses, crystal structure and properties of [Cu(L) (benzoylformate)]X. *Inorg. Chim. Acta.* **1997**, *263*, 301–307.
24. Nicoson, J. S.; Wang, L.; Becker, R. H.; Huff Hartz, K. E.; Muller, C. E.; Margerum, D. W. Kinetics and Mechanisms of the Ozone/Bromite and Ozone/Chlorite Reactions. *Inorg. Chem.* **2002**, *41*, 2975–2980.
25. Buxton, G. V. D. F. S. The Radiolysis of Aqueous Solutions of Oxybromine Compounds; The Spectra and Reactions of BrO and BrO_2. *Proc. R. Soc. London, A* **1968**, *304*, 427–439.